Coupling ferromagnetic and antiferromagnetic dynamics via phonons

Majid Shirdel-Havar and Babak Zare Rameshti [*]

Department of Physics, Iran University of Science and Technology, Narmak, Tehran 16844, Iran

We predict a coherent nonlocal coupling of ferromagnetic and antiferromagnetic magnetization dynamics via transverse phonon momentum current in a nonmagnetic insulator spacer. This coupling requires perpendicular alignment of magnetic moments to the phonon propagation direction. Our results bridge the divide between ferromagnetic and antiferromagnetic spintronics, offering pathways for integrating diverse magnetic elements into spintronic devices.

I. INTRODUCTION

The long-range transfer of spin angular momentum is a significant challenge in the development of spintronic devices. The nonlocal transport of spin in a ferromagnet [1,2] and an antiferromagnet [3] via magnons, the collective excitations of the magnet, has been observed over the micrometer scale. Phonons, the collective excitations of lattice vibration, can also serve as carriers of spin angular momentum [4–7], providing an additional mechanism for spin propagation. Due to their inherent low acoustic damping, phonons can carry spin angular momentum over distances that surpass the decay length of magnons [4–7]. Magnetoelastic coupling (MEC) in the strong-coupling regime leads to the formation of magnon polarons [5,8–10], which can affect the spin and thermal transport properties of magnetic insulators [11–15].

Magnetization dynamics in a magnetic insulator excite transverse acoustic phonons, which propagate into an adjacent nonmagnetic (NM) layer, carrying spin angular momentum [4,16,17]. This phonon pumping creates an extra loss channel for magnetization dynamics [4], similar to the enhanced damping from spin pumping into an attached normal metal [18,19]. Recent experimental [16,20] and theoretical investigations [16,17,21–25] have provided compelling evidence of spin angular momentum propagation across NM insulators via phonons over micrometer and sub-millimeter length scales. The propagation of spin-carrying phonons through a NM insulator enables the coherent and long-range coupling of magnetization in distant magnetic insulators, as observed in ferromagnetic resonance (FMR) experiments [16], where the emergence of bright and dark states is determined by the parity of the phonon modes [20]. A dynamic coupling between distant ferromagnets via attenuating elastic waves, offering long-distance synchronization and non-Hermitian manipulation of magnonic modes, has been proposed [26].

The coupling of magnons to optical [27,28] and acoustic phonons [29–33] due to the MEC in antiferromagnetic (AFM) insulators has been studied. An anomalous feature detected in the spin Seebeck response of an AFM insulator [29,30] and predicted in nonlocal spin current [31] is attributed to magnon-polaron formation. The nonlocal spin transport setup has also revealed a characteristic length scale for magnon-polaron formation in antiferromagnets [31]. Consequently, the phonon pumping into an attached NM layer is anticipated to be accompanied by spin angular momentum transfer.

Here we predict a nonlocal and coherent coupling between ferromagnetic (FM) and AFM insulators over macroscopic distances through phonons transmitted via a NM insulator. Despite the distinct characteristics of FM and AFM magnons, they couple through the same phonon mode of the NM insulator, acting as a phonon waveguide. Magnons in the antiferromagnet are converted into phonons which can then be transferred to the distant ferromagnet and vice versa, detectable by FMR and antiferromagnetic resonance (AFMR) measurements. Notably, this nonlocal magnon-magnon coupling occurs when the magnetic moments in the ferromagnet and the antiferromagnet are perpendicular to the phonon propagation direction, with a coupling strength comparable to that observed between two ferromagnets [16]. A nonlocal coupling mediated by cavity photons between two FM magnons [34] and between FM and AFM magnons were demonstrated [35]. The coupling via cavity photons is limited by the significant difference in velocities of light and magnons, which restricts the coupling of the cavity to magnons with zero wave vector. Moreover, the weak interaction between antiferromagnetic and magnetic fields, due to the vanishing magnetization of the antiferromagnet, may hinder efficient coupling with the cavity. This work heralds the integration of diverse magnetic materials, propelling AFM spintronics alongside established FM components.

This paper is organized as follows. Section II investigates nonlocal coupling between FM and AFM layers via phonons, and Sec. III establishes the theoretical framework for magnetization dynamics in the FM and AFM insulators coupled to a NM material. Section IV presents our findings on the realization of nonlocal phonon-mediated coupling between the FM and AFM layers. In Sec. V, we conclude and summarize our findings.
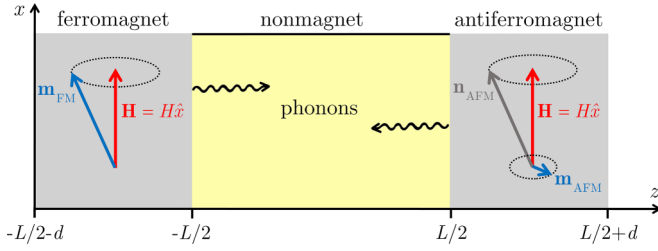
[*]bzarer@iust.ac.ir

FIG. 1. Schematic of the setup. A NM elastic layer of thickness L separates insulating FM and AFM layers of equal thickness d. $\mathbf{H}$ denotes the static external magnetic field in the x direction. $\mathbf{m}_{\mathrm{FM}}$ and $\mathbf{m}_{\mathrm{AFM}}$ represent the magnetization of FM and AFM layers, respectively, while $\mathbf{n}_{\mathrm{AFM}}$ is the Néel order parameter.

II. CONFIGURATION

We consider a heterostructure comprising insulating FM and uniaxial AFM layers of equal thickness d, separated by a NM insulator of length L, as depicted in Fig. 1. The FM layer has a single right-handed magnon mode, while the uniaxial AFM layer has both right- and left-handed magnon modes. When aligning the magnetic moments with the phonon propagation direction (the z axis), the FM and AFM right-handed magnons, sharing the same polarization, couple to a circularly polarized acoustic phonon mode of the same polarization. However, the frequency mismatch hinders nonlocal coupling between ferromagnet and antiferromagnet through this phonon mode. The FM magnon mode and AFM left-handed magnon mode, despite potentially having the same frequency, couple to the same phonon modes but with independent polarizations due to their opposite spins, preventing nonlocal magnon-magnon coupling. A viable solution could involve reversing the applied field to one of the FM or AFM layers, enabling coupling to the same phonon mode with the same polarization.

To enable nonlocal coupling between FM and AFM magnon modes, the magnetic moments should align perpendicular to the phonon propagation direction, along the x axis. This configuration breaks the rotational symmetry and allows for equal coupling of magnons to both polarizations of the phonon mode, viz., effectively coupling to a linearly polarized phonon mode. Linearly polarized acoustic phonons can interact with magnons of opposite spins, enabling a nonlocal coupling between the FM magnon mode and the AFM left-handed magnon mode. Unlike their circularly polarized counterparts, linearly polarized phonons do not carry net angular momentum [6,7]. Hence, our focus is on this specific configuration, as illustrated in Fig 1.

III. THEORETICAL DESCRIPTION

We assume that a bias magnetic field is applied to both ferromagnet and antiferromagnet perpendicular to the phonon propagation direction, along the x axis. The magnetization dynamics of ferromagnet is governed by the Landau-Lifshitz-Gilbert (LLG) equation:

$$\dot{\mathbf{m}}_{\mathrm{FM}} = -\gamma\mu_0\mathbf{m}_{\mathrm{FM}} \times \mathbf{H}_{\mathrm{FM}}^{\mathrm{eff}} + \alpha_{\mathrm{FM}}^{\mathrm{G}}\mathbf{m}_{\mathrm{FM}} \times \dot{\mathbf{m}}_{\mathrm{FM}}, \quad (1)$$

where $\mathbf{m}_{\mathrm{FM}} = \mathbf{M}_{\mathrm{FM}}/M_{s,\mathrm{FM}}$ is the magnetization vector normalized by the saturated magnetization $M_{s,\mathrm{FM}}$, γ is the gyromagnetic ratio, and $\alpha_{\mathrm{FM}}^{\mathrm{G}}$ is the Gilbert damping constant. The effective magnetic field $\mathbf{H}_{\mathrm{FM}}^{\mathrm{eff}}$ combines the contributions of $\mathbf{H}_{\mathrm{FM}}^{\mathrm{mag}}$, which includes the external magnetic field $\mathbf{H}^{\mathrm{ext}}$, magnetostatic and anisotropy fields, and $\mathbf{H}_{\mathrm{FM}}^{\mathrm{mec}}$ arising from the MEC. The external magnetic field consists of a static component $H\hat{\mathbf{x}}$ parallel to the in-plane x direction and perpendicular to the surface normal, along with a small dynamic component $\mathbf{h}_{y,z}(t)$ oscillating in the yz plane. Thus, $\mathbf{H}_{\mathrm{FM}}^{\mathrm{mag}}$ can be expressed as

$$\mathbf{H}_{\mathrm{FM}}^{\mathrm{mag}} = \frac{1}{\gamma\mu_0}[\omega_{\mathrm{H}}\hat{\mathbf{x}} - \omega_{\mathrm{M}}(\mathbf{m}_{\mathrm{FM}})_z\hat{\mathbf{z}}] + \mathbf{h}_{y,z}(t), \quad (2)$$

with $\omega_{\mathrm{H}} = \gamma\mu_0[H - 2K_{\mathrm{FM}}/(\mu_0 M_{s,\mathrm{FM}})]$ and $\omega_{\mathrm{M}} = \gamma\mu_0 M_{s,\mathrm{FM}}$, where K_{FM} is the anisotropy constant. The MEC field can be expressed as $\mathbf{H}_{\mathrm{FM}}^{\mathrm{mec}} = -\nabla_{\mathbf{m}_{\mathrm{FM}}} E_{\mathrm{FM}}^{\mathrm{mec}}/(\mu_0 V M_{s,\mathrm{FM}})$, where V is the volume of the ferromagnet and $E_{\mathrm{FM}}^{\mathrm{mec}}$ is the MEC energy for the FM layer, which reads

$$E_{\mathrm{FM}}^{\mathrm{mec}} = 2\sum_{\alpha\geqslant\beta}B_{\alpha\beta}\int_V m_{\mathrm{FM},\alpha}(\mathbf{r})m_{\mathrm{FM},\beta}(\mathbf{r})S_{\alpha\beta}(\mathbf{r})dV, \quad (3)$$

where $S_{\alpha\beta}(\mathbf{r}) = [\partial R_\beta(\mathbf{r})/\partial r_\alpha + \partial R_\alpha(\mathbf{r})/\partial r_\beta]/2$ is the strain tensor with $\mathbf{R}(\mathbf{r})$ being the lattice displacement field, $B_{\alpha\beta} = \delta_{\alpha\beta}B_\parallel + (1 - \delta_{\alpha\beta})B_\perp$ denotes the MEC coefficients for a cubic lattice [36], and $\alpha, \beta = x, y, z$. The magnetization vector of the FM layer, around its equilibrium configuration, is expanded as $\mathbf{m}_{\mathrm{FM}} = \hat{\mathbf{x}} + \delta\mathbf{m}_{\mathrm{FM}}$, where $\delta\mathbf{m}_{\mathrm{FM}} = \delta m_{\mathrm{FM},y}\hat{\mathbf{y}} + \delta m_{\mathrm{FM},z}\hat{\mathbf{z}}$. Hence, the MEC energy $E_{\mathrm{FM}}^{\mathrm{mec}}$ for the FM layer can be written as

$$E_{\mathrm{FM}}^{\mathrm{mec}} = B_{\perp,\mathrm{FM}}A\delta m_{\mathrm{FM},z}\left[R_x\left(-\frac{L}{2}\right) - R_x\left(-\frac{L}{2} - d\right)\right], \quad (4)$$

where $B_{\perp,\mathrm{FM}}$ represents the off-diagonal MEC coefficient of the FM layer, and A denotes the cross-sectional area. The MEC energy is derived under the assumption of a uniform lattice displacement field, $R_\alpha(\mathbf{r}) = R_\alpha(z)$. This approximation is considered valid for generating phonons through magnetization dynamics in thin layers, where the thickness is much smaller than the cross-sectional area, i.e., $d \ll \sqrt{A}$. The MEC field thus reads

$$\mathbf{H}_{\mathrm{FM}}^{\mathrm{mec}} = -\frac{\omega_{\mathrm{FM}}^{\mathrm{mec}}}{\gamma\mu_0 d}\mathcal{R}_{\mathrm{FM}}\hat{\mathbf{z}}, \quad (5)$$

with $\omega_{\mathrm{FM}}^{\mathrm{mec}} = \gamma B_{\perp,\mathrm{FM}}/M_{s,\mathrm{FM}}$ and $\mathcal{R}_{\mathrm{FM}} = [R_x(-L/2) - R_x(-L/2 - d)]$.

Substituting $\mathbf{H}_{\mathrm{FM}}^{\mathrm{eff}}$ and $\mathbf{m}_{\mathrm{FM}}$ in Eq. (1), and considering the leading order in the small dynamic fields, yields

$$\delta\dot{m}_{\mathrm{FM},y} = -(\omega_{\mathrm{H}} + \omega_{\mathrm{M}})\delta m_{\mathrm{FM},z} - \alpha_{\mathrm{FM}}^{\mathrm{G}}\delta\dot{m}_{\mathrm{FM},z}$$
$$+ \mathfrak{h}_z - \frac{\omega_{\mathrm{FM}}^{\mathrm{mec}}}{d}\mathcal{R}_{\mathrm{FM}}, \quad (6\mathrm{a})$$

$$\delta\dot{m}_{\mathrm{FM},z} = \omega_{\mathrm{H}}\delta m_{\mathrm{FM},y} + \alpha_{\mathrm{FM}}^{\mathrm{G}}\delta\dot{m}_{\mathrm{FM},y} - \mathfrak{h}_y, \quad (6\mathrm{b})$$

where $\mathfrak{h}_{y(z)} \equiv \gamma\mu_0 h_{y(z)}$.

The exchange-coupled bipartite antiferromagnet consists of two magnetic sublattices, denoted as a and b, with

antialigned magnetic moments $\mathbf{M}_a$ and $\mathbf{M}_b$, respectively, where $|\mathbf{M}_a| \approx |\mathbf{M}_b| \equiv M_s$, with M_s being the saturation magnetization of each sublattice. In the long-wavelength limit, the average magnetization is given by $\mathbf{M}_{\mathrm{AFM}} = (\mathbf{M}_a + \mathbf{M}_b)/2 = M_s \mathbf{m}_{\mathrm{AFM}}$ and the AFM order parameter is expressed as $\mathbf{L}_{\mathrm{AFM}} = (\mathbf{M}_a - \mathbf{M}_b)/2 = M_s \mathbf{n}_{\mathrm{AFM}}$, where $\mathbf{m}_{\mathrm{AFM}}$ and $\mathbf{n}_{\mathrm{AFM}}$ represent the dimensionless average magnetization and the Néel order vectors, and describes the magnetic state of the antiferromagnet [37–41]. Below the Néel temperature $\mathbf{m}_{\mathrm{AFM}} \cdot \mathbf{n}_{\mathrm{AFM}} = 0$ and $\mathbf{m}_{\mathrm{AFM}}^2 + \mathbf{n}_{\mathrm{AFM}}^2 = 1$ [39,41]. The magnetization dynamics of antiferromagnet is governed by the LLG equation as

$$\dot{\mathbf{m}}_{\mathrm{AFM}} = -\gamma\mu_0\big(\mathbf{m}_{\mathrm{AFM}} \times \mathbf{H}_{m_{\mathrm{AFM}}}^{\mathrm{eff}} + \mathbf{n}_{\mathrm{AFM}} \times \mathbf{H}_{n_{\mathrm{AFM}}}^{\mathrm{eff}}\big)$$
$$+ \alpha_{\mathrm{AFM}}^{\mathrm{G}}(\mathbf{m}_{\mathrm{AFM}} \times \dot{\mathbf{m}}_{\mathrm{AFM}} + \mathbf{n}_{\mathrm{AFM}} \times \dot{\mathbf{n}}_{\mathrm{AFM}}), \quad (7\mathrm{a})$$

$$\dot{\mathbf{n}}_{\mathrm{AFM}} = -\gamma\mu_0\big(\mathbf{m}_{\mathrm{AFM}} \times \mathbf{H}_{n_{\mathrm{AFM}}}^{\mathrm{eff}} + \mathbf{n}_{\mathrm{AFM}} \times \mathbf{H}_{m_{\mathrm{AFM}}}^{\mathrm{eff}}\big)$$
$$+ \alpha_{\mathrm{AFM}}^{\mathrm{G}}(\mathbf{m}_{\mathrm{AFM}} \times \dot{\mathbf{n}}_{\mathrm{AFM}} + \mathbf{n}_{\mathrm{AFM}} \times \dot{\mathbf{m}}_{\mathrm{AFM}}), \quad (7\mathrm{b})$$

the effective magnetic field for $\mathbf{m}_{\mathrm{AFM}}(\mathbf{n}_{\mathrm{AFM}})$ is given by $\mathbf{H}_{m_{\mathrm{AFM}}(n_{\mathrm{AFM}})}^{\mathrm{eff}} = \mathbf{H}_{m_{\mathrm{AFM}}(n_{\mathrm{AFM}})}^{\mathrm{mag}} + \mathbf{H}_{m_{\mathrm{AFM}}(n_{\mathrm{AFM}})}^{\mathrm{mec}}$, where $\mathbf{H}_{m_{\mathrm{AFM}}(n_{\mathrm{AFM}})}^{\mathrm{mec}}$ is the MEC field and $\mathbf{H}_{m_{\mathrm{AFM}}(n_{\mathrm{AFM}})}^{\mathrm{mag}} = -\nabla_{\mathbf{m}_{\mathrm{AFM}}(\mathbf{n}_{\mathrm{AFM}})}E_{\mathrm{AFM}}^{\mathrm{mag}}/(\mu_0 V M_{s,\mathrm{AFM}})$. Here $M_{s,\mathrm{AFM}} = 2M_s$ represents the total saturated magnetization of the antiferromagnet with volume V. The damping of $\mathbf{m}_{\mathrm{AFM}}$ and $\mathbf{n}_{\mathrm{AFM}}$ are chosen to be the same and denoted by $\alpha_{\mathrm{AFM}}^{\mathrm{G}}$. The magnetic free energy for the antiferromagnet, $E_{\mathrm{AFM}}^{\mathrm{mag}}$, which incorporates the exchange interaction, anisotropy, and the external magnetic field energies, reads

$$E_{\mathrm{AFM}}^{\mathrm{mag}} = \frac{M_{s,\mathrm{AFM}}}{\gamma} \int \bigg(\frac{\xi}{2}\mathbf{m}_{\mathrm{AFM}}^2 + \frac{\nu}{2}[\nabla\mathbf{n}_{\mathrm{AFM}}]^2$$
$$- \gamma\mu_0\mathbf{H}^{\mathrm{ext}} \cdot \mathbf{m}_{\mathrm{AFM}} - \frac{K_{\mathrm{AFM}}}{2}(n_{\mathrm{AFM},x})^2\bigg)dV. \quad (8)$$

Here ξ and ν are the inter- and intra-sublattice exchange constants, respectively, and K_{AFM} is the uniaxial anisotropy constant taken along the x axis. Hence the corresponding effective field $\mathbf{H}_{m_{\mathrm{AFM}}(n_{\mathrm{AFM}})}^{\mathrm{mag}}$ can be obtained as

$$\mathbf{H}_{m_{\mathrm{AFM}}}^{\mathrm{mag}} = -\frac{\xi}{\gamma\mu_0}\mathbf{m}_{\mathrm{AFM}} + \mathbf{n}_{\mathrm{AFM}} \times (\mathbf{H}^{\mathrm{ext}} \times \mathbf{n}_{\mathrm{AFM}}), \quad (9\mathrm{a})$$

$$\mathbf{H}_{n_{\mathrm{AFM}}}^{\mathrm{mag}} = \frac{\nu}{\gamma\mu_0}\nabla^2\mathbf{n}_{\mathrm{AFM}} - \mathbf{m}_{\mathrm{AFM}}(\mathbf{H}^{\mathrm{ext}} \cdot \mathbf{n}_{\mathrm{AFM}}) + \frac{K_{\mathrm{AFM}}}{\gamma\mu_0}n_{\mathrm{AFM},x}\hat{\mathbf{x}}. \quad (9\mathrm{b})$$

The Néel order parameter of the antiferromagnet interacts with the lattice displacement field, resulting in the corresponding MEC energy:

$$E_{\mathrm{AFM}}^{\mathrm{mec}} = 2\sum_{\alpha \geqslant \beta} B_{\alpha\beta}\int_V n_{\mathrm{AFM},\alpha}(\mathbf{r})n_{\mathrm{AFM},\beta}(\mathbf{r})S_{\alpha\beta}(\mathbf{r})dV. \quad (10)$$

The magnetization and Néel vectors of the AFM layer around the equilibrium configuration, i.e., $\mathbf{n}_{\mathrm{AFM}} = \pm\hat{\mathbf{x}}$ and $\mathbf{m}_{\mathrm{AFM}} \approx 0$, can be expanded as $\mathbf{m}_{\mathrm{AFM}} = \delta\mathbf{m}_{\mathrm{AFM}}$ and $\mathbf{n}_{\mathrm{AFM}} = \hat{\mathbf{x}} + \delta\mathbf{n}_{\mathrm{AFM}}$, where $\delta\mathbf{m}_{\mathrm{AFM}} = \delta m_{\mathrm{AFM},y}\hat{\mathbf{y}} + \delta m_{\mathrm{AFM},z}\hat{\mathbf{z}}$ and $\delta\mathbf{n}_{\mathrm{AFM}} = \delta n_{\mathrm{AFM},y}\hat{\mathbf{y}} + \delta n_{\mathrm{AFM},z}\hat{\mathbf{z}}$. The MEC energy for the antiferromagnet then simplifies to

$$E_{\mathrm{AFM}}^{\mathrm{mec}} = B_{\perp,\mathrm{AFM}}A\delta n_{\mathrm{AFM},z}\bigg[R_x\bigg(\frac{L}{2}+d\bigg) - R_x\bigg(\frac{L}{2}\bigg)\bigg], \quad (11)$$

with $B_{\perp,\mathrm{AFM}}$ being the off-diagonal MEC coefficient of the AFM layer, yielding the respective effective fields

$$\mathbf{H}_{m_{\mathrm{AFM}}}^{\mathrm{mec}} = 0, \quad (12\mathrm{a})$$

$$\mathbf{H}_{n_{\mathrm{AFM}}}^{\mathrm{mec}} = -\frac{\omega_{\mathrm{AFM}}^{\mathrm{mec}}}{\gamma\mu_0 d}\mathcal{R}_{\mathrm{AFM}}\hat{\mathbf{z}}, \quad (12\mathrm{b})$$

with $\omega_{\mathrm{AFM}}^{\mathrm{mec}} = \gamma B_{\perp,\mathrm{AFM}}/M_{s,\mathrm{AFM}}$ and $\mathcal{R}_{\mathrm{AFM}} = [R_x(L/2 + d) - R_x(L/2)]$.

By incorporating $\mathbf{H}_{m_{\mathrm{AFM}}(n_{\mathrm{AFM}})}^{\mathrm{eff}}$, $\mathbf{m}_{\mathrm{AFM}}$, and $\mathbf{n}_{\mathrm{AFM}}$ into Eqs. (7a) and (7b), the LLG equation can be linearized as

$$\delta\dot{m}_{\mathrm{AFM},y} = -(K_{\mathrm{AFM}} - \nu\nabla^2)\delta n_{\mathrm{AFM},z} - H_0\delta m_{\mathrm{AFM},z}$$
$$- \alpha_{\mathrm{AFM}}^{\mathrm{G}}\delta\dot{n}_{\mathrm{AFM},z} - \frac{\omega_{\mathrm{AFM}}^{\mathrm{mec}}}{d}\mathcal{R}_{\mathrm{AFM}}, \quad (13\mathrm{a})$$

$$\delta\dot{m}_{\mathrm{AFM},z} = (K_{\mathrm{AFM}} - \nu\nabla^2)\delta n_{\mathrm{AFM},y} + H_0\delta m_{\mathrm{AFM},y}$$
$$+ \alpha_{\mathrm{AFM}}^{\mathrm{G}}\delta\dot{n}_{\mathrm{AFM},y}, \quad (13\mathrm{b})$$

$$\delta\dot{n}_{\mathrm{AFM},y} = -(K_{\mathrm{AFM}} + \xi)\delta m_{\mathrm{AFM},z} - H_0\delta n_{\mathrm{AFM},z}$$
$$- \alpha_{\mathrm{AFM}}^{\mathrm{G}}\delta\dot{m}_{\mathrm{AFM},z} + \mathfrak{h}_z, \quad (13\mathrm{c})$$

$$\delta\dot{n}_{\mathrm{AFM},z} = (K_{\mathrm{AFM}} + \xi)\delta m_{\mathrm{AFM},y} + H_0\delta n_{\mathrm{AFM},y}$$
$$+ \alpha_{\mathrm{AFM}}^{\mathrm{G}}\delta\dot{m}_{\mathrm{AFM},y} - \mathfrak{h}_y, \quad (13\mathrm{d})$$

where $H_0 \equiv \gamma\mu_0 H$. Moreover, R_x can be derived from the elastic equations of motion for an isotropic medium, given by

$$p_x(z,t) = \rho(z)\dot{R}_x(z,t), \quad (14\mathrm{a})$$

$$\dot{p}_x(z,t) = \mu(z)\nabla_z^2 R_x(z,t) - 2\eta(z)p_x(z,t), \quad (14\mathrm{b})$$

where $p_x(z,t)$ represents the transverse momentum density, and $\rho(z)$, $\mu(z)$, and $\eta(z)$ are the mass density, shear modulus, and elastic damping constant, respectively. In the FM(AFM) layer, these parameters are given by $\rho(z) = \rho_{\mathrm{FM(AFM)}}$, $\mu(z) = \mu_{\mathrm{FM(AFM)}} = \rho_{\mathrm{FM(AFM)}}c_{\mathrm{FM(AFM)}}^2$, and $\eta(z) = \eta_{\mathrm{FM(AFM)}}$, while in the NM spacer, they are $\tilde{\rho}$, $\tilde{\mu} = \tilde{\rho}\tilde{c}^2$, and $\tilde{\eta}$, with $c_{\mathrm{FM(AFM)}}$ and $\tilde{c}$ as the transverse sound velocities in the magnetic and NM layers, respectively. Now, solving the elastic equations of motion yields

$$R_x(z,t) = \begin{cases} A(\omega)e^{ik_{\mathrm{FM}}z-i\omega t} + B(\omega)e^{-ik_{\mathrm{FM}}z-i\omega t}, & -d-L/2 < z < -L/2, \\ C(\omega)e^{i\tilde{k}z-i\omega t} + D(\omega)e^{-i\tilde{k}z-i\omega t}, & -L/2 < z < L/2, \\ E(\omega)e^{ik_{\mathrm{AFM}}z-i\omega t} + F(\omega)e^{-ik_{\mathrm{AFM}}z-i\omega t}, & L/2 < z < L/2+d, \end{cases} \quad (15)$$

where $k_{\text{FM(AFM)}} = \sqrt{\omega^2 + 2i\omega\eta_{\text{FM(AFM)}}}/c_{\text{FM(AFM)}}$ and $\tilde{k} = \sqrt{\omega^2 + 2i\omega\tilde{\eta}}/\tilde{c}$ are the phonon wave vectors of the FM(AFM) layer and the NM spacer, respectively. The coefficients $A(\omega), \dots, F(\omega)$ are determined by satisfying the elastic continuity and momentum conservation boundary conditions.

The phonon pumping to the attached nonmagnet generates a transverse momentum current at the FM(AFM)|nonmagnet boundaries, given by $j_x(z) = -\mu(z)\partial R_x(z)/\partial z$. This momentum current is related to the transverse momentum p_x by $\dot{p}_x(z) = -\partial j_x(z)/\partial z$. The momentum current density is driven by surface shear forces $\mathbf{N}(\equiv \dot{\mathbf{p}}V) = -\nabla_{R_\alpha(z)}E_{\text{FM(AFM)}}^{\text{mec}}$ at the boundaries

$$N_x(-L/2-d) = -N_x(-L/2) = B_{\perp,\text{FM}}A\delta m_{\text{FM},z},$$
$$N_x(L/2) = -N_x(L/2+d) = B_{\perp,\text{AFM}}A\delta n_{\text{AFM},z}. \quad (16)$$

The elastic continuity at the FM|NM interface and momentum conservation at the boundaries of ferromagnet can be written as

$$R_x(-L/2^+) = R_x(-L/2^-),$$
$$j_x(-L/2-d^+) = B_{\perp,\text{FM}}\delta m_{\text{FM},z},$$
$$j_x(-L/2^+) - j_x(-L/2^-) = -B_{\perp,\text{FM}}\delta m_{\text{FM},z}, \quad (17)$$

with corresponding boundary conditions at the AFM interfaces

$$R_x(L/2^+) = R_x(L/2^-),$$
$$j_x(L/2^-) - j_x(L/2^+) = -B_{\perp,\text{AFM}}\delta n_{\text{AFM},z},$$
$$j_x(L/2+d^-) = B_{\perp,\text{AFM}}\delta n_{\text{AFM},z}. \quad (18)$$

The coefficients $A(\omega), \dots, F(\omega)$, determined by the boundary conditions, can be expressed as linear combinations of $\delta m_{\text{FM},z}$ and $\delta n_{\text{AFM},z}$ as $A(\omega) = \mathcal{A}_1(\omega)\delta m_{\text{FM},z} + \mathcal{A}_2(\omega)\delta n_{\text{AFM},z}, \dots, F(\omega) = \mathcal{F}_1(\omega)\delta m_{\text{FM},z} + \mathcal{F}_2(\omega)\delta n_{\text{AFM},z}$. The analytical solutions for $\mathcal{A}_1, \dots, \mathcal{F}_2$ are presented in Appendix A. Consequently, the expressions for $\mathcal{R}_{\text{FM}}$ and $\mathcal{R}_{\text{AFM}}$ in Eqs. (6a) and (13a) are obtained as

$$\mathcal{R}_{\text{FM}} = \Omega_1\delta m_{\text{FM},z} + \Omega_2\delta n_{\text{AFM},z}, \quad (19)$$

$$\mathcal{R}_{\text{AFM}} = \Psi_1\delta m_{\text{FM},z} + \Psi_2\delta n_{\text{AFM},z}, \quad (20)$$

with

$$\Omega_{1(2)} = 2i\sin(k_{\text{FM}}d/2)$$
$$\times [\mathcal{A}_{1(2)}e^{-ik_{\text{FM}}(L+d)/2} - \mathcal{B}_{1(2)}e^{ik_{\text{FM}}(L+d)/2}], \quad (21a)$$
$$\Psi_{1(2)} = 2i\sin(k_{\text{AFM}}d/2)$$
$$\times [\mathcal{E}_{1(2)}e^{ik_{\text{AFM}}(L+d)/2} - \mathcal{F}_{1(2)}e^{-ik_{\text{AFM}}(L+d)/2}]. \quad (21b)$$

The detailed derivation of the coupled dynamics for the FM and AFM layers is provided in Appendix B.

The microwave power absorption P^{abs} is an observable in FMR/AFMR experiments and can be utilized as a probe for nonlocal magnon-magnon coupling. We study P^{abs} by FM and AFM layers when an external dynamical magnetic field $\mathbf{h}_{y,z}(t) = e^{-i\omega t}(h_y\hat{\mathbf{y}} + h_z\hat{\mathbf{z}})$ is applied in the yz plane and perpendicular to H. The power absorption is given by [16,42]

$$P_{\text{FM(AFM)}}^{\text{abs}}(H,\omega) \propto \kappa_{\text{FM(AFM)}}\text{Im}(\mathfrak{h}_y^\star\delta m_y + \mathfrak{h}_z^\star\delta m_z)_{\text{FM(AFM)}}, \quad (22)$$

where $\kappa_{\text{FM(AFM)}}$ is the inductive coupling of FM(AFM) with microwave antenna (see Appendix B), and $\star$ denotes the complex conjugate.

IV. RESULTS AND DISCUSSION

Having obtained the solutions for the coupled magnetoelastic dynamics, we compute observables that quantify the long-range coupling between the FM and AFM materials mediated by phonons. Yttrium iron garnet (YIG) and NaNiO$_2$ are chosen as the FM and AFM materials, respectively, both with thicknesses of $d = 200$ nm. Gadolinium gallium garnet (GGG) is used as the NM spacer with a thickness of $L = 0.25$ mm. We use the following parameters for these three materials. For YIG, $\mu_0 M_{s,\text{FM}} = 0.1720$ T, $\rho_{\text{FM}} = 5170$ Kg/m^3, $\alpha_{\text{FM}}^{\text{G}} = 9 \times 10^{-5}$, $B_{\perp,\text{FM}} = 6.96 \times 10^5$ J/m^3, $c_{\text{FM}} = 3843$ m/s, and $K_{\text{FM}} = -6.1 \times 10^2$ J/m^3 [16,17,43]. For NaNiO$_2$, $\mu_0 M_{s,\text{AFM}} = 0.580$ T [35], $K_{\text{AFM}} = 62$ GHz, $\xi = 1.68$ THz [44], $\rho_{\text{AFM}} = 4600$ Kg/m^3, $\alpha_{\text{AFM}}^{\text{G}} = 10^{-4}$, $B_{\perp,\text{AFM}} \approx 16.5 \times 10^5$ J/m^3, and $c_{\text{AFM}} = 3900$ m/s. To the best of our knowledge, the magnetoelastic coefficient for NaNiO$_2$ remains undetermined. Therefore, we estimated $B_{\perp,\text{AFM}}$ based on values reported for similar magnetic materials [45,46]. For GGG, $\tilde{\rho} = 7070$ Kg/m^3, and $\tilde{c} = 3530$ m/s [47]. The phonon damping is taken to be equal throughout this heterostructure, $\eta_{\text{FM,AFM}} = \tilde{\eta} = 0.35 \times 2\pi \times 10^6$ rad/s [16,21].

By neglecting the small Gilbert damping, the magnon modes of ferromagnet and antiferromagnet can be determined as follows:

$$[\omega^2 - \omega_{\text{FMR}}^2]\delta m_{\text{FM},y(z)} = 0, \quad (23)$$

$$[\omega^2 - (\sqrt{K_{\text{AFM}}(K_{\text{AFM}}+\xi)} \pm H_0)^2]\delta m_{\text{AFM},y(z)} = 0. \quad (24)$$

The FMR mode, depicted by the solid line in Fig. 2(a) is observable at $\omega = \omega_{\text{FMR}} = \sqrt{\omega_{\text{H}}(\omega_{\text{H}} + \omega_{\text{M}})}$. The AFM right-handed (RH) and left-handed (LH) magnon modes, represented by $\omega = \sqrt{K_{\text{AFM}}(K_{\text{AFM}}+\xi)} \pm H_0$, are denoted as $\omega_{\text{AFMR}}^{\text{RH}}$ and $\omega_{\text{AFMR}}^{\text{LH}}$, respectively. These modes are shown as dashed lines in Fig. 2(a). Notably, for magnetic fields below the spin-flop field, i.e., $H < H_{\text{SF}} = \sqrt{K_{\text{AFM}}(K_{\text{AFM}}+\xi)}/(\gamma\mu_0)$, coupling between the FMR and LH AFMR modes occurs due to their interaction with the same phonon modes.

The microwave absorption spectra of the FM and AFM layers, obtained by varying the bias magnetic field and frequency, are plotted in Fig. 2(b). The absorption spectra of the FMR and AFMR modes, as described by Eqs. (23) and (24), undergo frequency modulation due to their interaction with a sequence of standing phonon modes.

Assuming that the acoustic impedances are matched [$\rho_{\text{FM(AFM)}}c_{\text{FM(AFM)}} \approx \tilde{\rho}\tilde{c}$], which is valid at GHz frequencies where the acoustic mismatch, $\rho_{\text{FM}}c_{\text{FM}}/\tilde{\rho}\tilde{c} \approx 0.8$ and $\rho_{\text{AFM}}c_{\text{AFM}}/\tilde{\rho}\tilde{c} \approx 0.72$, is irrelevant, the acoustic resonance frequencies are given by

$$\frac{\omega_n^{\text{ph}}}{2\pi} = \frac{n}{2(d/c_{\text{FM}} + d/c_{\text{AFM}} + L/\tilde{c})}, \quad (25)$$
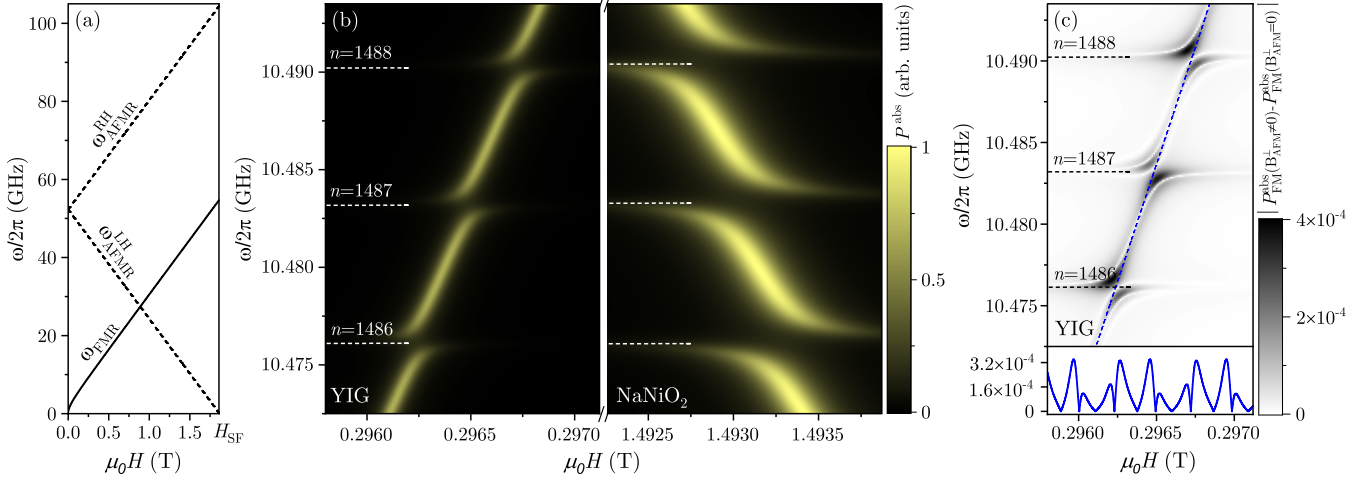
FIG. 2. (a) FMR mode (solid line) in YIG and left- and right-hand AFMR modes (dashed lines) in NaNiO$_2$ as a function of magnetic field. (b) The absorption spectrum as a function of probe frequency and applied field near the FMR mode in YIG (left panel) and the left-hand AFMR mode in NaNiO$_2$ (right panel). (c) The contrast in FMR absorption $|P_{FM}^{abs}(B_{\perp,AFM} \neq 0) - P_{FM}^{abs}(B_{\perp,AFM} = 0)|$ due to constructive/destructive interference between FM and AFM layer dynamics. The bottom panel displays the intensity modulation along the blue dashed line, which represents a cut parallel to the FMR mode. YIG and NaNiO$_2$ are $d = 200$ nm thick, separated by GGG with $L = 0.25$ mm. Here $\kappa_{AFM}/\kappa_{FM} = 7$, which is chosen to be close to the experiment [16].

which in the limit of $L \gg d$ further simplifies to $\omega_n^{ph}/2\pi \approx \tilde{c}/\lambda_n^{ph}$, where $\lambda_n^{ph} = 2(2d+L)/n$ represents the wavelength of standing acoustic waves formed across the total thickness $2d + L$ with n being the phonon mode number (see Appendix A). The periodicity of 7 MHz in Fig. 2(b) can be attributed to the equidistant splitting of standing phonon modes, i.e., $(\omega_{n+1}^{ph} - \omega_n^{ph})/2\pi = \tilde{c}/2(2d+L) \approx 7$ MHz. The level repulsion between phonon and magnon modes that occurs at $\omega_{FMR/AFMR} = \omega_n^{ph}$ represents a strong coupling between phonons and magnons and leads to the formation of magnon polarons. Typically, magnons at frequency of $\omega_{FMR(AFMR)}/2\pi \approx 10.476$ GHz (according to a magnetic field of $\mu_0 H \approx 0.2962$ T for YIG and $\mu_0 H \approx 1.4933$ T for NaNiO$_2$) couple to an even phonon mode with mode number $n \approx 1486$, corresponding to an acoustic phonon wavelength of $\lambda_n^{ph} \approx 337$ nm.

The phonons pumped by the dynamics of each magnetic layer transmit transverse momentum current across the 0.25-mm thickness of GGG, with a characteristic decay length of $\delta = \tilde{c}/\tilde{\eta} \approx 1.6$ mm. Depending on the parity of the mode number n (odd or even), the magnetization dynamics in one layer either absorb or reflect the phononic momentum current pumped from the other layer. This leads to constructive or destructive interference between the magnetization dynamics in FM and AFM layers mediated by even or odd phonon modes, resulting in a distinct power absorption contrast determined by the ratio of microwave field amplitudes experienced by each magnetic layer κ_{AFM}/κ_{FM}.

The magnetic absorption modulation, $|P_{FM}^{abs}(B_{\perp,AFM} \neq 0) - P_{FM}^{abs}(B_{\perp,AFM} = 0)|$, resulting from the indirect coupling mediated by the phonon between two magnetic layers, is shown in Fig. 2(c). The FM absorption signal exhibits a periodicity of 7 MHz, featuring a contrast in P_{FM}^{abs} between consecutive phonon modes. The absorption modulation along the blue dashed line, representing a cut parallel to the FMR

mode, is depicted in the bottom panel of Fig. 2(c). Similar interference effects have been observed in an FM|NM|FM system, through the dynamics of ferromagnet employing the inverse spin Hall voltage [20] and via absorption power measurement with a microwave antenna [16,20]. These effects are anticipated to manifest in the FM|NM|AFM system via FM/AFM dynamics, using similar techniques.

We present the eigenmodes of the coupled magnetoelastic dynamics in Fig. 3(a), to assess the nonlocal coupling strength between FM and AFM magnons. Here we focus on a dispersive regime, where the phonon mode's frequency is slightly off-resonant with the crossing point of FM and AFM magnons ($\omega_{FMR} = \omega_{AFMR}^{LH}$). This allows us to determine the strength of the phonon-mediated magnon-magon coupling. We select
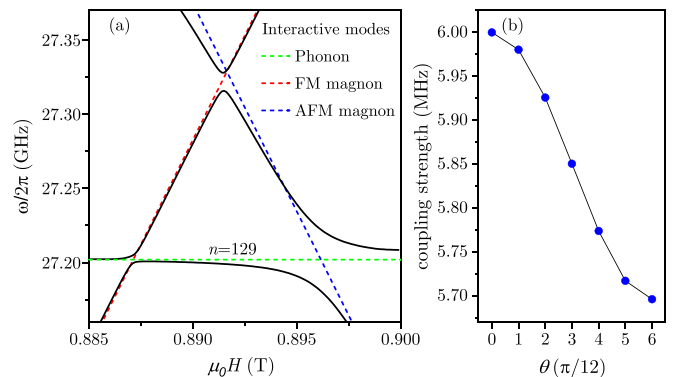

FIG. 3. (a) The eigenmodes of the coupled YIG and NaNiO$_2$ dynamics, depicted with dashed and solid lines representing dispersion relations without and with MEC, respectively. YIG and NaNiO$_2$ are both 200 nm thick, while GGG has a thickness of 8 μm. (b) The angular dependency of indirect coupling strength between YIG and NaNiO$_2$ dynamics, with θ denoting the angle between the external magnetic field applied to the FM layer and the x axis in the xy plane.

the $n = 129$ phonon mode with a frequency of $\omega_{129}^{\text{ph}}/(2\pi) \simeq 27.20$ GHz positioned below the crossing point of the FM and AFM magnon modes. The coupling strengths between this phonon mode and the FM and AFM magnon modes are 2.7 and 20 MHz, respectively. The level repulsion between FM and AFM magnon modes at their crossing point indicates the nonlocal magnon-magnon coupling via coherent acoustic phonon modes, leading to the formation of an eigenstate that is a linear superposition of both magnons. The strength of the phonon-mediated coupling, determined by the splitting at the nominal crossing point, is 6 MHz. This coupling strength is comparable to that observed between two YIG films [16,26]. The shifts in both FM and AFM magnon modes in the interacting system, compared to the noninteracting system, depend on the coupling strength with phonons. AFM magnons shift more than FM magnons, due to their stronger coupling with phonons.

The variation in nonlocal coupling strength between FM and AFM layers with the angle between the external magnetic field applied to the FM layer and the x axis within the xy plane is shown in Fig. 3(b). The maximum and minimum coupling strengths occur at 0 and $\pi/2$, respectively, corresponding to

the external field being parallel to the x and y axes. The decrease in nonlocal coupling strength is attributed to the reduced coupling of FM magnons with phonons.

V. CONCLUSIONS

In summary, our study unveils a phonon-mediated coupling mechanism that enables coherent long-range magnetization control between FM and AFM layers, separated by a NM spacer. This coupling relies on the perpendicular alignment of magnetic moments with the phonon propagation direction and is mediated by phononic transverse momentum currents, resulting in magnetic power absorption contrasts and level repulsion in collective modes. These findings have significant implications for future spintronic devices and advance our understanding of magnon-phonon interactions.

APPENDIX A: DERIVATION OF LATTICE DISPLACEMENT FIELD

Here, we calculate the lattice displacement coefficients in Eq. (15). By substituting the lattice displacement R_x and the transverse momentum current j_x into the boundary conditions given by Eqs. (17) and (18), we end up with

$$Ae^{-ik_{\text{FM}}L/2} + Be^{ik_{\text{FM}}L/2} = Ce^{-i\tilde{k}L/2} + De^{i\tilde{k}L/2},$$

$$[Be^{ik_{\text{FM}}(L/2+d)} - Ae^{-ik_{\text{FM}}(L/2+d)}] = \frac{B_{\perp,\text{FM}}\delta m_{\text{FM},z}}{\mu_{\text{FM}}ik_{\text{FM}}},$$

$$\tilde{\mu}i\tilde{k}[De^{i\tilde{k}L/2} - Ce^{-i\tilde{k}L/2}] + \mu_{\text{FM}}ik_{\text{FM}}[Ae^{-ik_{\text{FM}}L/2} - Be^{ik_{\text{FM}}L/2}] = -B_{\perp,\text{FM}}\delta m_{\text{FM},z},$$

$$Ce^{i\tilde{k}L/2} + De^{-i\tilde{k}L/2} = Ee^{ik_{\text{AFM}}L/2} + Fe^{-ik_{\text{AFM}}L/2},$$

$$\mu_{\text{AFM}}ik_{\text{AFM}}[Ee^{ik_{\text{AFM}}L/2} - Fe^{-ik_{\text{AFM}}L/2}] + \tilde{\mu}i\tilde{k}[De^{-i\tilde{k}L/2} - Ce^{i\tilde{k}L/2}] = -B_{\perp,\text{AFM}}\delta n_{\text{AFM},z},$$

$$[Fe^{-ik_{\text{AFM}}(L/2+d)} - Ee^{ik_{\text{AFM}}(L/2+d)}] = \frac{B_{\perp,\text{AFM}}\delta n_{\text{AFM},z}}{\mu_{\text{AFM}}ik_{\text{AFM}}}. \tag{A1}$$

By solving these equations, the coefficients $A(\omega), \dots, F(\omega)$ are determined as linear combinations of $\delta m_{\text{FM},z}$ and $\delta n_{\text{AFM},z}$ expressed as $A(\omega) = \mathcal{A}_1(\omega)\delta m_{\text{FM},z} + \mathcal{A}_2(\omega)\delta n_{\text{AFM},z}, \dots, F(\omega) = \mathcal{F}_1(\omega)\delta m_{\text{FM},z} + \mathcal{F}_2(\omega)\delta n_{\text{AFM},z}$, with $\mathcal{A}_1, \dots, \mathcal{F}_2$ given below:

$$\mathcal{A}_1 = \frac{iB_{\perp,\text{FM}}e^{ik_{\text{FM}}L/2}}{2\mathcal{L}\mu_{\text{FM}}k_{\text{FM}}}\{e^{i\tilde{k}L}\mathcal{J}_2^-[\tilde{\mu}i\tilde{k} - 2\mu_{\text{FM}}k_{\text{FM}}e^{ik_{\text{FM}}d/2}\sin(k_{\text{FM}}d/2)] - e^{-i\tilde{k}L}\mathcal{J}_2^+[\tilde{\mu}i\tilde{k} + 2\mu_{\text{FM}}k_{\text{FM}}e^{ik_{\text{FM}}d/2}\sin(k_{\text{FM}}d/2)]\}, \tag{A2a}$$

$$\mathcal{A}_2 = -2\tilde{\mu}i\tilde{k}B_{\perp,\text{AFM}}e^{ik_{\text{FM}}(L/2+d)}\sin^2(k_{\text{AFM}}d/2)/\mathcal{L}, \tag{A2b}$$

$$\mathcal{B}_1 = \frac{iB_{\perp,\text{FM}}e^{-ik_{\text{FM}}L/2}}{2\mathcal{L}\mu_{\text{FM}}k_{\text{FM}}}\{-e^{i\tilde{k}L}\mathcal{J}_2^-[\tilde{\mu}i\tilde{k} - 2\mu_{\text{FM}}k_{\text{FM}}e^{-ik_{\text{FM}}d/2}\sin(k_{\text{FM}}d/2)] + e^{-i\tilde{k}L}\mathcal{J}_2^+[\tilde{\mu}i\tilde{k} + 2\mu_{\text{FM}}k_{\text{FM}}e^{-ik_{\text{FM}}d/2}\sin(k_{\text{FM}}d/2)]\}, \tag{A2c}$$

$$\mathcal{B}_2 = -2\tilde{\mu}i\tilde{k}B_{\perp,\text{AFM}}e^{-ik_{\text{FM}}(L/2+d)}\sin^2(k_{\text{AFM}}d/2)/\mathcal{L}, \tag{A2d}$$

$$\mathcal{C}_1 = 2B_{\perp,\text{FM}}e^{-i\tilde{k}L/2}\sin^2(k_{\text{FM}}d/2)\mathcal{J}_2^+/\mathcal{L}, \tag{A2e}$$

$$\mathcal{C}_2 = -2B_{\perp,\text{AFM}}e^{i\tilde{k}L/2}\sin^2(k_{\text{AFM}}d/2)\mathcal{J}_1^-/\mathcal{L}, \tag{A2f}$$

$$\mathcal{D}_1 = 2B_{\perp,\text{FM}}e^{i\tilde{k}L/2}\sin^2(k_{\text{FM}}d/2)\mathcal{J}_2^-/\mathcal{L}, \tag{A2g}$$

$$\mathcal{D}_2 = -2B_{\perp,\text{AFM}}e^{-i\tilde{k}L/2}\sin^2(k_{\text{AFM}}d/2)\mathcal{J}_1^+/\mathcal{L}, \tag{A2h}$$

$$\mathcal{E}_1 = 2\tilde{\mu}i\tilde{k}B_{\perp,\text{FM}}e^{-ik_{\text{AFM}}(L/2+d)}\sin^2(k_{\text{FM}}d/2)/\mathcal{L}, \tag{A2i}$$

$$\mathcal{E}_2 = \frac{-iB_{\perp,\mathrm{AFM}}e^{-ik_{\mathrm{AFM}}L/2}}{2\mathcal{L}\mu_{\mathrm{AFM}}k_{\mathrm{AFM}}}\{-e^{i\tilde{k}L}\mathcal{J}_1^-[\tilde{\mu}i\tilde{k} - 2\mu_{\mathrm{AFM}}k_{\mathrm{AFM}}e^{-ik_{\mathrm{AFM}}d/2}\sin(k_{\mathrm{AFM}}d/2)]$$

$$+ e^{-i\tilde{k}L}\mathcal{J}_1^+[\tilde{\mu}i\tilde{k} + 2\mu_{\mathrm{AFM}}k_{\mathrm{AFM}}e^{-ik_{\mathrm{AFM}}d/2}\sin(k_{\mathrm{AFM}}d/2)]\}, \tag{A2j}$$

$$\mathcal{F}_1 = 2\tilde{\mu}i\tilde{k}B_{\perp,\mathrm{FM}}e^{ik_{\mathrm{AFM}}(L/2+d)}\sin^2(k_{\mathrm{FM}}d/2)/\mathcal{L}, \tag{A2k}$$

$$\mathcal{F}_2 = \frac{-iB_{\perp,\mathrm{AFM}}e^{ik_{\mathrm{AFM}}L/2}}{2\mathcal{L}\mu_{\mathrm{AFM}}k_{\mathrm{AFM}}}\{e^{i\tilde{k}L}\mathcal{J}_1^-[\tilde{\mu}i\tilde{k} - 2\mu_{\mathrm{AFM}}k_{\mathrm{AFM}}e^{ik_{\mathrm{AFM}}d/2}\sin(k_{\mathrm{AFM}}d/2)]$$

$$- e^{-i\tilde{k}L}\mathcal{J}_1^+[\tilde{\mu}i\tilde{k} + 2\mu_{\mathrm{AFM}}k_{\mathrm{AFM}}e^{ik_{\mathrm{AFM}}d/2}\sin(k_{\mathrm{AFM}}d/2)]\}, \tag{A2l}$$

where

$$\mathcal{J}_1^+ = \tilde{\mu}i\tilde{k}\cos(k_{\mathrm{FM}}d) + \mu_{\mathrm{FM}}k_{\mathrm{FM}}\sin(k_{\mathrm{FM}}d), \tag{A3a}$$

$$\mathcal{J}_1^- = \tilde{\mu}i\tilde{k}\cos(k_{\mathrm{FM}}d) - \mu_{\mathrm{FM}}k_{\mathrm{FM}}\sin(k_{\mathrm{FM}}d), \tag{A3b}$$

$$\mathcal{J}_2^+ = \tilde{\mu}i\tilde{k}\cos(k_{\mathrm{AFM}}d) + \mu_{\mathrm{AFM}}k_{\mathrm{AFM}}\sin(k_{\mathrm{AFM}}d), \tag{A3c}$$

$$\mathcal{J}_2^- = \tilde{\mu}i\tilde{k}\cos(k_{\mathrm{AFM}}d) - \mu_{\mathrm{AFM}}k_{\mathrm{AFM}}\sin(k_{\mathrm{AFM}}d), \tag{A3d}$$

$$\mathcal{L} = e^{i\tilde{k}L}\mathcal{J}_1^-\mathcal{J}_2^- - e^{-i\tilde{k}L}\mathcal{J}_1^+\mathcal{J}_2^+. \tag{A3e}$$

The acoustic resonance condition can be obtained as follows:

$$\cos(\tilde{k}L)\left[\frac{Z_{\mathrm{AFM}}}{\tilde{Z}}\cos(k_{\mathrm{FM}}d)\sin(k_{\mathrm{AFM}}d) + \frac{Z_{\mathrm{FM}}}{\tilde{Z}}\cos(k_{\mathrm{AFM}}d)\sin(k_{\mathrm{FM}}d)\right]$$

$$+ \sin(\tilde{k}L)\left[\cos(k_{\mathrm{FM}}d)\cos(k_{\mathrm{AFM}}d) - \frac{Z_{\mathrm{FM}}Z_{\mathrm{AFM}}}{\tilde{Z}^2}\sin(k_{\mathrm{FM}}d)\sin(k_{\mathrm{AFM}}d)\right] = 0, \tag{A4}$$

where $Z_{\mathrm{FM(AFM)}} = \rho_{\mathrm{FM(AFM)}}c_{\mathrm{FM(AFM)}}$ and $\tilde{Z} = \tilde{\rho}\tilde{c}$. When the acoustic impedances are matched, $Z_{\mathrm{FM(AFM)}} = \tilde{Z}$, the resonance condition is given by $k_{\mathrm{FM}}d + k_{\mathrm{AFM}}d + \tilde{k}L = n\pi$, with $n = 1, 2, \ldots$ corresponding to the formation of standing waves [21]. The acoustic resonance frequencies are then given by Eq. (25).

To investigate the resonance condition in more detail, the coefficient $|\mathcal{A}_1(\omega)|$ is plotted in Fig. 4 as a function of $\tilde{k}L$ for $\omega = \omega_{\mathrm{FMR}} = 66.5\,\mathrm{GHz}$ and various values of $k_{\mathrm{FM}}d = k_{\mathrm{AFM}}d = (0.5, 1, 2, 3)\pi$. As can be seen, the resonance occurs at $\tilde{k}L = q\pi$ when $k_{\mathrm{FM(AFM)}}d$ equals either $(2p+1)\pi/2$ or $(2p+1)\pi$, where $q = 1, 2, \ldots$ and $p = 0, 1, \ldots$, consistent with Eq. (25). As a result, the phonon excitation is suppressed for $d = 2p\lambda_n^{\mathrm{ph}}/2$, which is in agreement with Refs. [16,21], and favored for $d = (2p+1)\lambda_n^{\mathrm{ph}}/2$. Under the condition $k_{\mathrm{FM}}d = k_{\mathrm{AFM}}d = (2p+1)\pi$ and matched acoustic impedances $Z_{\mathrm{FM(AFM)}} = \tilde{Z}$, the coefficients $\mathcal{A}_1, \ldots, \mathcal{F}_2$ are then simplified as

$$\mathcal{A}_1 = \frac{B_{\perp,\mathrm{FM}}e^{ik_{\mathrm{FM}}L/2}}{2\tilde{\mu}\tilde{k}\sin(\tilde{k}L)}[2\cos(\tilde{k}L) - i\sin(\tilde{k}L)], \tag{A5a}$$

$$\mathcal{A}_2 = -B_{\perp,\mathrm{AFM}}e^{ik_{\mathrm{FM}}L/2}/[\tilde{\mu}\tilde{k}\sin(\tilde{k}L)], \tag{A5b}$$

$$\mathcal{B}_1 = \frac{B_{\perp,\mathrm{FM}}e^{-ik_{\mathrm{FM}}L/2}}{2\tilde{\mu}\tilde{k}\sin(\tilde{k}L)}[2\cos(\tilde{k}L) + i\sin(\tilde{k}L)], \tag{A5c}$$

$$\mathcal{B}_2 = -B_{\perp,\mathrm{AFM}}e^{-ik_{\mathrm{FM}}L/2}/[\tilde{\mu}\tilde{k}\sin(\tilde{k}L)], \tag{A5d}$$

$$\mathcal{C}_1 = B_{\perp,\mathrm{FM}}e^{i\tilde{k}L/2}/[\tilde{\mu}\tilde{k}\sin(\tilde{k}L)], \tag{A5e}$$

$$\mathcal{C}_2 = -B_{\perp,\mathrm{AFM}}e^{i\tilde{k}L/2}/[\tilde{\mu}\tilde{k}\sin(\tilde{k}L)], \tag{A5f}$$

$$\mathcal{D}_1 = B_{\perp,\mathrm{FM}}e^{i\tilde{k}L/2}/[\tilde{\mu}\tilde{k}\sin(\tilde{k}L)], \tag{A5g}$$

$$\mathcal{D}_2 = -B_{\perp,\mathrm{AFM}}e^{-i\tilde{k}L/2}/[\tilde{\mu}\tilde{k}\sin(\tilde{k}L)], \tag{A5h}$$

$$\mathcal{E}_1 = B_{\perp,\mathrm{FM}}e^{-ik_{\mathrm{AFM}}L/2}/[\tilde{\mu}\tilde{k}\sin(\tilde{k}L)], \tag{A5i}$$

$$\mathcal{E}_2 = -\frac{B_{\perp,\mathrm{AFM}}e^{-ik_{\mathrm{AFM}}L/2}}{2\tilde{\mu}\tilde{k}\sin(\tilde{k}L)}[2\cos(\tilde{k}L) + i\sin(\tilde{k}L)], \tag{A5j}$$

$$\mathcal{F}_1 = B_{\perp,\mathrm{FM}}e^{ik_{\mathrm{AFM}}L/2}/[\tilde{\mu}\tilde{k}\sin(\tilde{k}L)], \tag{A5k}$$

$$\mathcal{F}_2 = -\frac{B_{\perp,\mathrm{AFM}}e^{ik_{\mathrm{AFM}}L/2}}{2\tilde{\mu}\tilde{k}\sin(\tilde{k}L)}[2\cos(\tilde{k}L) - i\sin(\tilde{k}L)]. \tag{A5l}$$

When $\tilde{Z} \gg Z_{\mathrm{FM(AFM)}}$ and assuming $k_{\mathrm{FM}} \approx k_{\mathrm{AFM}} = k$, the acoustic resonance condition, Eq. (A4), becomes

$$\frac{Z}{\tilde{Z}}\cos(\tilde{k}L)\sin(2kd) + \sin(\tilde{k}L)\cos^2(kd) = 0, \tag{A6}$$

where $Z = Z_{\mathrm{FM}} \approx Z_{\mathrm{AFM}}$. For $\tilde{k}L = q\pi$, the acoustic resonances occur at $2kd = (2p+1)\pi$, which agrees with Refs. [4,48].

APPENDIX B: THE COUPLED EQUATIONS OF MOTION

We provide the detailed derivation of linearized equations of motion for magnetoelastic dynamics, allowing to one determine both the dispersion relation of the interacting system and the power absorption of the magnetic layers. Substituting $\mathcal{R}_{\mathrm{FM}}$ and $\mathcal{R}_{\mathrm{AFM}}$ into Eqs. (6a) and (13a), followed by taking the time derivative of Eqs. (6) and (13) while
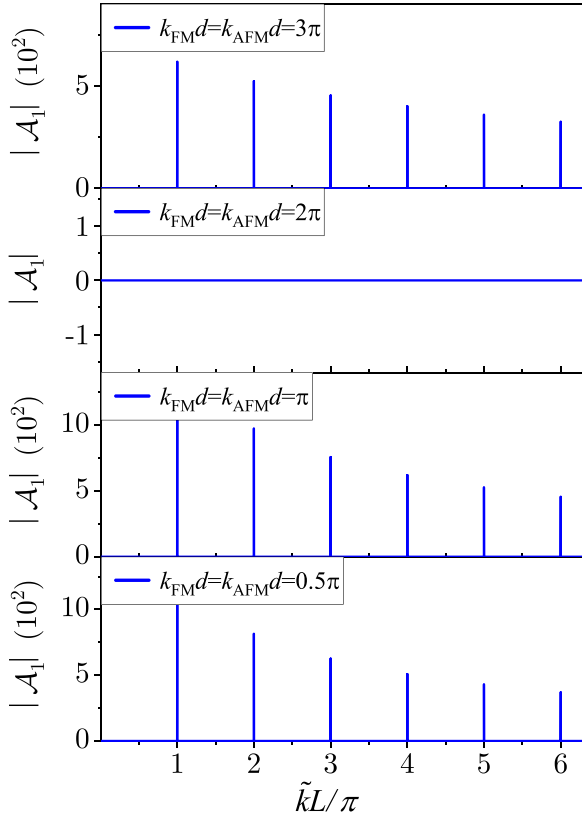
FIG. 4. The coefficient $|\mathcal{A}_1(\omega)|$ as a function of $\tilde{k}L$ for $\omega = \omega_{\text{FMR}} = 66.5$ GHz and various values of $k_{\text{FM}}d = k_{\text{AFM}}d = (0.5, 1, 2, 3)\pi$. Here, $Z_{\text{FM}}/\tilde{Z} \approx 0.8$ and $Z_{\text{AFM}}/\tilde{Z} \approx 0.72$.

neglecting terms proportional to $(\alpha_{\text{FM(AFM)}}^{\text{G}})^2$, yields the coupled frequency-domain equations of motion:

$$M_{11}\delta m_{\text{FM},y} + M_{12}\delta m_{\text{AFM},y} + M_{13}\delta n_{\text{AFM},y} = \mathcal{P}_1, \quad \text{(B1a)}$$

$$M_{21}\delta m_{\text{FM},y} + M_{22}\delta m_{\text{AFM},y} + M_{23}\delta n_{\text{AFM},y} = \mathcal{P}_2, \quad \text{(B1b)}$$

$$M_{32}\delta m_{\text{AFM},y} + M_{33}\delta n_{\text{AFM},y} = \mathcal{P}_3, \quad \text{(B1c)}$$

$$N_{11}\delta m_{\text{FM},z} + N_{13}\delta n_{\text{AFM},z} = \mathcal{S}_1, \quad \text{(B1d)}$$

$$N_{21}\delta m_{\text{FM},z} + N_{22}\delta m_{\text{AFM},z} + N_{23}\delta n_{\text{AFM},z} = \mathcal{S}_2, \quad \text{(B1e)}$$

$$N_{31}\delta m_{\text{FM},z} + N_{32}\delta m_{\text{AFM},z} + N_{33}\delta n_{\text{AFM},z} = \mathcal{S}_3, \quad \text{(B1f)}$$

where

$$M_{11} = \omega^2 + \left(2\omega_{\text{H}} + \omega_{\text{M}} + \frac{\omega_{\text{FM}}^{\text{mec}}}{d}\Omega_1\right)i\omega\alpha_{\text{FM}}^{\text{G}}$$
$$- \frac{\omega_{\text{H}}\omega_{\text{FM}}^{\text{mec}}}{d}\Omega_1 - \omega_{\text{FMR}}^2,$$

$$M_{12} = -\frac{\omega_{\text{FM}}^{\text{mec}}}{d}\left(K_{\text{AFM}} + \xi - i\omega\alpha_{\text{AFM}}^{\text{G}}\right)\Omega_2,$$

$$M_{13} = -\frac{H_0\omega_{\text{FM}}^{\text{mec}}}{d}\Omega_2,$$

$$M_{21} = \frac{\omega_{\text{AFM}}^{\text{mec}}}{d}\left(i\omega\alpha_{\text{FM}}^{\text{G}} - \omega_{\text{H}}\right)\Psi_1,$$

$$M_{22} = \omega^2 - \left(K_{\text{AFM}} - \nu\nabla^2 + \frac{\omega_{\text{AFM}}^{\text{mec}}}{d}\Psi_2\right)$$
$$\times \left(K_{\text{AFM}} + \xi - i\omega\alpha_{\text{AFM}}^{\text{G}}\right)$$
$$+ (K_{\text{AFM}} + \xi)i\omega\alpha_{\text{AFM}}^{\text{G}} - H_0^2,$$

$$M_{23} = -2\left(K_{\text{AFM}} - \nu\nabla^2 + \frac{\omega_{\text{AFM}}^{\text{mec}}}{2d}\Psi_2 - i\omega\alpha_{\text{AFM}}^{\text{G}}\right)H_0,$$

$$M_{32} = -2\left(K_{\text{AFM}} + \xi - i\omega\alpha_{\text{AFM}}^{\text{G}}\right)H_0,$$

$$M_{33} = \omega^2 - \left(K_{\text{AFM}} - \nu\nabla^2\right)\left(K_{\text{AFM}} + \xi - i\omega\alpha_{\text{AFM}}^{\text{G}}\right)$$
$$+ (K_{\text{AFM}} + \xi)i\omega\alpha_{\text{AFM}}^{\text{G}} - H_0^2,$$

$$\mathcal{P}_1 = \left(i\omega\alpha_{\text{FM}}^{\text{G}} - \omega_{\text{H}} - \omega_{\text{M}} - \frac{\omega_{\text{FM}}^{\text{mec}}}{d}\Omega_1\right)\mathfrak{h}_y$$
$$- \frac{\omega_{\text{FM}}^{\text{mec}}}{d}\Omega_2\mathfrak{h}_y + i\omega\mathfrak{h}_z,$$

$$\mathcal{P}_2 = -\left(K_{\text{AFM}} - \nu\nabla^2 + \frac{\omega_{\text{AFM}}^{\text{mec}}}{d}\Psi_2 - i\omega\alpha_{\text{AFM}}^{\text{G}}\right)\mathfrak{h}_y$$
$$- \frac{\omega_{\text{AFM}}^{\text{mec}}}{d}\Psi_1\mathfrak{h}_y,$$

$$\mathcal{P}_3 = -H_0\mathfrak{h}_y + i\omega\mathfrak{h}_z,$$

$$N_{11} = \omega^2 + \left(2\omega_{\text{H}} + \omega_{\text{M}} + \frac{\omega_{\text{FM}}^{\text{mec}}}{d}\Omega_1\right)i\omega\alpha_{\text{FM}}^{\text{G}}$$
$$- \frac{\omega_{\text{H}}\omega_{\text{FM}}^{\text{mec}}}{d}\Omega_1 - \omega_{\text{FMR}}^2,$$

$$N_{13} = \frac{\omega_{\text{FM}}^{\text{mec}}}{d}\left(i\omega\alpha_{\text{FM}}^{\text{G}} - \omega_{\text{H}}\right)\Omega_2,$$

$$N_{21} = -\frac{H_0\omega_{\text{AFM}}^{\text{mec}}}{d}\Psi_1,$$

$$N_{22} = \omega^2 - \left(K_{\text{AFM}} - \nu\nabla^2\right)\left(K_{\text{AFM}} + \xi - i\omega\alpha_{\text{AFM}}^{\text{G}}\right)$$
$$+ (K_{\text{AFM}} + \xi)i\omega\alpha_{\text{AFM}}^{\text{G}} - H_0^2,$$

$$N_{23} = -2\left(K_{\text{AFM}} - \nu\nabla^2 + \frac{\omega_{\text{AFM}}^{\text{mec}}}{2d}\Psi_2 - i\omega\alpha_{\text{AFM}}^{\text{G}}\right)H_0,$$

$$N_{31} = -\frac{\omega_{\text{AFM}}^{\text{mec}}}{d}\left(K_{\text{AFM}} + \xi - i\omega\alpha_{\text{AFM}}^{\text{G}}\right)\Psi_1,$$

$$N_{32} = -2H_0\left(K_{\text{AFM}} + \xi - i\omega\alpha_{\text{AFM}}^{\text{G}}\right),$$

$$N_{33} = \omega^2 - \left(K_{\text{AFM}} - \nu\nabla^2 + \frac{\omega_{\text{AFM}}^{\text{mec}}}{d}\Psi_2\right)$$
$$\times \left(K_{\text{AFM}} + \xi - i\omega\alpha_{\text{AFM}}^{\text{G}}\right)$$
$$+ (K_{\text{AFM}} + \xi)i\omega\alpha_{\text{AFM}}^{\text{G}} - H_0^2,$$

$$\mathcal{S}_1 = \left(i\omega\alpha_{\text{FM}}^{\text{G}} - \omega_{\text{H}}\right)\mathfrak{h}_z - i\omega\mathfrak{h}_y,$$

$$\mathcal{S}_2 = -\left(K_{\text{AFM}} - \nu\nabla^2 - i\omega\alpha_{\text{AFM}}^{\text{G}}\right)\mathfrak{h}_z,$$

$$\mathcal{S}_3 = -H_0\mathfrak{h}_z - i\omega\mathfrak{h}_y. \quad \text{(B2)}$$

Equations (B.1) reveal the coupled dynamics of FM and AFM layers through MEC.

Equation (B1c) allows solving for $\delta n_{\text{AFM},y}$, which, when inserted into Eqs. (B1a) and (B1b), results in

$$\begin{pmatrix} \delta m_{\text{FM},y} \\ \delta m_{\text{AFM},y} \end{pmatrix} = \chi \begin{pmatrix} \mathcal{P}_1 - \mathcal{P}_3 M_{13}/M_{33} \\ \mathcal{P}_2 - \mathcal{P}_3 M_{23}/M_{33} \end{pmatrix}, \qquad \text{(B3)}$$

in which χ is the susceptibility tensor

$$\chi^{-1} = \begin{pmatrix} M_{11} & M_{12} - M_{13}M_{32}/M_{33} \\ M_{21} & M_{22} - M_{23}M_{32}/M_{33} \end{pmatrix}, \qquad \text{(B4)}$$

and similarly for Eqs. (B1d)–(B1f), we get

$$\begin{pmatrix} \delta m_{\text{FM},z} \\ \delta m_{\text{AFM},z} \end{pmatrix} = \chi \begin{pmatrix} \mathcal{S}_1 - \mathcal{S}_3 N_{13}/N_{33} \\ \mathcal{S}_2 - \mathcal{S}_3 N_{23}/N_{33} \end{pmatrix}, \qquad \text{(B5)}$$

where

$$\chi^{-1} = \begin{pmatrix} N_{11} - N_{13}N_{31}/N_{33} & -N_{13}N_{32}/N_{33} \\ N_{21} - N_{23}N_{31}/N_{33} & N_{22} - N_{23}N_{32}/N_{33} \end{pmatrix}. \qquad \text{(B6)}$$

[1] L. Cornelissen, J. Liu, R. Duine, J. B. Youssef, and B. Van Wees, Nat. Phys. **11**, 1022 (2015).

[2] L. J. Cornelissen and B. J. van Wees, Phys. Rev. B **93**, 020403(R) (2016).

[3] R. Lebrun, A. Ross, S. Bender, A. Qaiumzadeh, L. Baldrati, J. Cramer, A. Brataas, R. Duine, and M. Kläui, Nature (London) **561**, 222 (2018).

[4] S. Streib, H. Keshtgar, and G. E. W. Bauer, Phys. Rev. Lett. **121**, 027202 (2018).

[5] J. Holanda, D. Maior, A. Azevedo, and S. Rezende, Nat. Phys. **14**, 500 (2018).

[6] J. J. Nakane and H. Kohno, Phys. Rev. B **97**, 174403 (2018).

[7] D. A. Garanin and E. M. Chudnovsky, Phys. Rev. B **92**, 024421 (2015).

[8] A. Kamra, H. Keshtgar, P. Yan, and G. E. W. Bauer, Phys. Rev. B **91**, 104409 (2015).

[9] S. Streib, N. Vidal-Silva, K. Shen, and G. E. W. Bauer, Phys. Rev. B **99**, 184442 (2019).

[10] B. Zare Rameshti and R. A. Duine, Phys. Rev. B **99**, 060402(R) (2019).

[11] H. Man, Z. Shi, G. Xu, Y. Xu, X. Chen, S. Sullivan, J. Zhou, K. Xia, J. Shi, and P. Dai, Phys. Rev. B **96**, 100406(R) (2017).

[12] T. Kikkawa, K. Shen, B. Flebus, R. A. Duine, K. I. Uchida, Z. Qiu, G. E. W. Bauer, and E. Saitoh, Phys. Rev. Lett. **117**, 207203 (2016).

[13] L. J. Cornelissen, K. Oyanagi, T. Kikkawa, Z. Qiu, T. Kuschel, G. E. W. Bauer, B. J. van Wees, and E. Saitoh, Phys. Rev. B **96**, 104441 (2017).

[14] B. Flebus, K. Shen, T. Kikkawa, K.-I. Uchida, Z. Qiu, E. Saitoh, R. A. Duine, and G. E. W. Bauer, Phys. Rev. B **95**, 144420 (2017).

[15] R. Yahiro, T. Kikkawa, R. Ramos, K. Oyanagi, T. Hioki, S. Daimon, and E. Saitoh, Phys. Rev. B **101**, 024407 (2020).

[16] K. An, A. N. Litvinenko, R. Kohno, A. A. Fuad, V. V. Naletov, L. Vila, U. Ebels, G. de Loubens, H. Hurdequint, N. Beaulieu, J. Ben Youssef, N. Vukadinovic, G. E. W. Bauer, A. N. Slavin, V. S. Tiberkevich, and O. Klein, Phys. Rev. B **101**, 060407(R) (2020).

[17] T. Sato, W. Yu, S. Streib, and G. E. W. Bauer, Phys. Rev. B **104**, 014403 (2021).

[18] Y. Tserkovnyak, A. Brataas, and G. E. W. Bauer, Phys. Rev. Lett. **88**, 117601 (2002).

[19] A. Kapelrud and A. Brataas, Phys. Rev. Lett. **111**, 097602 (2013).

[20] K. An, R. Kohno, A. N. Litvinenko, R. L. Seeger, V. V. Naletov, L. Vila, G. de Loubens, J. Ben Youssef, N. Vukadinovic, G. E. W. Bauer, A. N. Slavin, V. S. Tiberkevich, and O. Klein, Phys. Rev. X **12**, 011060 (2022).

[21] A. Rückriegel and R. A. Duine, Phys. Rev. Lett. **124**, 117201 (2020).

[22] S. M. Rezende, D. S. Maior, O. Alves Santos, and J. Holanda, Phys. Rev. B **103**, 144430 (2021).

[23] X. Zhang, G. E. W. Bauer, and T. Yu, Phys. Rev. Lett. **125**, 077203 (2020).

[24] T. Yu, Phys. Rev. B **102**, 134417 (2020).

[25] O. Latcham, Y. Gusieva, A. Shytov, O. Gorobets, and V. Kruglyak, Appl. Phys. Lett. **115**, 082403 (2019).

[26] W. Yu, Phys. Rev. B **108**, 134414 (2023).

[27] Q. Zhang, M. Ozerov, E. V. Boström, J. Cui, N. Suri, Q. Jiang, C. Wang, F. Wu, K. Hwangbo, J.-H. Chu, D. Xiao, A. Rubio, and X. Xu, arXiv:2108.11619.

[28] H. T. Simensen, R. E. Troncoso, A. Kamra, and A. Brataas, Phys. Rev. B **99**, 064421 (2019).

[29] J. Li, H. T. Simensen, D. Reitz, Q. Sun, W. Yuan, C. Li, Y. Tserkovnyak, A. Brataas, and J. Shi, Phys. Rev. Lett. **125**, 217201 (2020).

[30] H. Liu and K. Shen, J. Appl. Phys. **131**, 103902 (2022).

[31] S. M. Tabatabaei, R. A. Duine, and B. Zare Rameshti, Phys. Rev. B **104**, 014432 (2021).

[32] J. Oh, M. D. Le, H.-H. Nahm, H. Sim, J. Jeong, T. Perring, H. Woo, K. Nakajima, S. Ohira-Kawamura, Z. Yamani et al., Nat. Commun. **7**, 13146 (2016).

[33] D. Vaclavkova, M. Palit, J. Wyzula, S. Ghosh, A. Delhomme, S. Maity, P. Kapuscinski, A. Ghosh, M. Veis, M. Grzeszczyk, C. Faugeras, M. Orlita, S. Datta, and M. Potemski, Phys. Rev. B **104**, 134437 (2021).

[34] B. Zare Rameshti and G. E. W. Bauer, Phys. Rev. B **97**, 014419 (2018).

[35] Ø. Johansen and A. Brataas, Phys. Rev. Lett. **121**, 087204 (2018).

[36] A. Rückriegel, P. Kopietz, D. A. Bozhko, A. A. Serga, and B. Hillebrands, Phys. Rev. B **89**, 184413 (2014).

[37] A. Borovik-Romanov and S. K. Sinha, *Spin Waves and Magnetic Excitations* (Elsevier, Amsterdam, 2012).

[38] A. N. Bogdanov, A. V. Zhuravlev, and U. K. Rößler, Phys. Rev. B **75**, 094425 (2007).

[39] O. Johansen and A. Brataas, Phys. Rev. B **95**, 220408(R) (2017).

[40] R. Cheng, J. Xiao, Q. Niu, and A. Brataas, Phys. Rev. Lett. **113**, 057601 (2014).

[41] O. Johansen, H. Skarsvåg, and A. Brataas, Phys. Rev. B **97**, 054423 (2018).

[42] S. M. Rezende, *Fundamentals of Magnonics*, Lecture Notes in Physics (Springer, Berlin 2020), Vol. 969.

[43] A. G. Gurevich and G. A. Melkov, *Magnetization Oscillations and Waves* (CRC, Boca Raton, FL, 1996).

[44] E. Chappel, M. Núñez-Regueiro, F. Dupont, G. Chouteau, C. Darie, and A. Sulpice, Eur. Phys. J. B **17**, 609 (2000).

[45] D. Fritsch and C. Ederer, Phys. Rev. B **86**, 014406 (2012).

[46] W. He, H. Huang, Z. Liu, and X. Ma, Chin. Phys. B **27**, 016201 (2018).

[47] Z. Kleszczewski and J. Bodzenta, Phys. Status Solidi B **146**, 467 (1988).

[48] M. Seavey, Proc. IEEE **53**, 1387 (1965).